# Competition among various charge-inhomogeneous states and *d*-wave superconducting state in Hubbard models on square lattices

Kota Ido, Takahiro Ohgoe, and Masatoshi Imada
*Department of Applied Physics, University of Tokyo, 7-3-1 Hongo, Bunkyo-ku, Tokyo 113-8656, Japan*

(Received 7 September 2017; revised manuscript received 14 December 2017; published 22 January 2018)

We study competitions among charge-uniform and -inhomogeneous states in two-dimensional Hubbard models by using a variational Monte Carlo method. At realistic parameters for cuprate superconductors, emergent effective attraction of carriers generated from repulsive Coulomb interaction leads to charge/spin stripe ground states, which severely compete with uniform superconducting excited states in the energy scale of 10 K for cuprates. Stripe period increases with decreasing hole doping $\delta$, which agrees with the experiments for La-based cuprates at $\delta = 1/8$. For lower $\delta$, we find a phase separation. Implications of the emergent attraction for cuprates are discussed.

DOI: 10.1103/PhysRevB.97.045138

## I. INTRODUCTION

After the discovery of the high-temperature superconductivity in the cuprates [1], its mechanism remains one of the most challenging issues in condensed-matter physics. A necessary condition of high-temperature superconductivity for strongly correlated electron systems is large effective attractive interactions between electronic carriers emerging from strong Coulomb repulsions. However, this strong attraction can also enhance the tendency of electron aggregations in real space. This means that the strong attractive interaction induces diverging charge compressibility [2,3] as well as charge-inhomogeneous states such as phase separations (PSs) and stripe states [4–16]. In fact, the competition between the superconductivity and the charge inhomogeneity as a stripe state has been observed and well discussed in La-based cuprates [17–21]. Recently, such phenomena were also reported in Y- [22–27], Hg- [23,28], and Bi-based cuprates [29–31], indicating a ubiquitous feature in the cuprate superconductors [32,33].

To understand the origin of superconductivity in cuprates, the Hubbard model on a square lattice has been studied for long time. Although many theoretical studies have been devoted to understanding the ground states of the Hubbard model, they are still under debate [2,12–15,34–46]. To gain insight into the charge-inhomogeneous phases including the stripes, detailed analyses of their existence and competitions with the *d*-wave superconductivity are desired, particularly on their dependences on the hole-doping concentration $\delta$, band structure, and the interaction. Most numerical studies based on variational calculations or dynamical mean-field theory showed that charge-uniform states are the ground states or macroscopic phase separation appears [12,13,35–37,40,41,47]. However, in these calculations, the possibility of long-period stripe states is ignored. Recent studies using the infinite projected entangled-pair states, the density-matrix embedding theory (DMET), the constrained-path auxiliary-field quantum Monte Carlo method, and the density-matrix renormalization group all reported the stripe ground state but studied systematically only for a special choice of band structure (only with nearest-neighbor transfer $t = 1$) at $\delta = 0.125$, with 8 and 16 periods for charge and spin stripes, respectively [46]. Recent variational Monte Carlo (VMC) calculations combined with tensor network states also found stripe states with 8 and 16 (for $\delta < 0.15$) and 4 and 8 (for $\delta > 0.15$) periods for charge and spin as ground states below $\delta \sim 0.25$ [15], respectively. However, the stripe period extensively studied at $\delta = 0.125$ in these calculations is different from that observed in La-based cuprates, which is four charge and eight spin periods [17,18]. These results imply that more systematic and realistic study is needed to understand the real cuprate systems.

One of the missing ingredients in the simple Hubbard model is hopping parameters beyond the nearest-neighbor pairs. The previous DMET study showed that the stripe state in the experiments has a lower energy than the charge-uniform state in the system with the next-nearest-neighbor hopping [43]. However, since the sizes of embedded clusters are restricted, the competitions with other stripe states are still unclear at a finite hole concentration.

In this paper, by using the VMC method, we study the competitions among stripe states with different periodicities in addition to charge-uniform states. We show that the ground states have stripe orders, the period of which decreases with increasing $\delta$ in a wide range. In the lower doping region, the PS occurs between the antiferromagnetic insulator and the stripe state. More importantly, we find that the stripe state experimentally observed at $\delta = 0.125$ is indeed the ground state for a realistic value of next-nearest-neighbor hopping. We clearly see that the superconducting (SC) long-range order is strongly suppressed due to the emergence of stripe orders, while charge-uniform and strong superconducting states exist as excited states with tiny excitation energies.

## II. MODEL AND METHOD

We study the $t - t'$ Hubbard model on square lattices under the antiperiodic-periodic boundary condition. The Hamiltonian is defined by

$$\mathcal{H} = -\sum_{i,j,\sigma} t_{ij} c^{\dagger}_{i\sigma} c_{j\sigma} + U \sum_{i}^{N_s} n_{i\uparrow} n_{i\downarrow}, \qquad (1)$$

 

where the hopping amplitude $t_{ij}$ is taken as $t_{ij} = t$ for the nearest-neighbor pairs, $t_{ij} = t'$ for the next-nearest-neighbor pairs, and otherwise $t_{ij} = 0$. $U$ is the on-site repulsive interaction, $N_s = L \times L$ is the system size, $c^\dagger_{i\sigma}$ ($c_{i\sigma}$) is a creation (annihilation) operator of an electron with spin $\sigma$ on site $i$, and $n_{i\sigma} = c^\dagger_{i\sigma} c_{i\sigma}$. The lattice constant is taken as the length unit. We mainly performed the calculations for $U/t = 10$ because it is close to the proposed *ab initio* estimate for cuprates [48].

To study the ground states of the Hubbard model, we have used the VMC method. As a trial wave function, we adopted the generalized pair-product wave function with correlation factors: $|\psi\rangle = \mathcal{P}_G \mathcal{P}_J \mathcal{P}^{\rm ex}_{\rm d-h} |\phi\rangle$ [49]. Here, the Gutzwiller factor $\mathcal{P}_G = \exp(-g \sum_i n_{i\uparrow} n_{i\downarrow})$, the Jastrow factor $\mathcal{P}_J = \exp(-\sum_{i,j} v_{ij} n_i n_j)$, and the doublon-holon correlation factor $\mathcal{P}^{\rm ex}_{\rm d-h} = \exp(-\sum_{m=0}^{5} \sum_{l=1,2} \alpha^{(l)}_{(m)} \sum_i \xi^{(l)}_{i(m)})$ are considered, and $|\phi\rangle = (\sum_{i,j}^{N_s} f_{ij} c^\dagger_{i\uparrow} c^\dagger_{j\downarrow})^{N/2} |0\rangle$, where $n_i = n_{i\uparrow} + n_{i\downarrow}$ and $N$ is the number of electrons. $\xi^{(l)}_{i(m)}$ is 1 when a doublon (holon) exists at the $i$th site and $m$ holons (doublons) surround the $l$th nearest neighbor. Otherwise, $\xi^{(l)}_{i(m)}$ is zero. In this study, we treat $g, v_{ij}, \alpha^{(l)}_{(m)}$, and $f_{ij}$ as variational parameters. To describe inhomogeneous stripe states, we assume that $f_{ij}$ has the $l_s \times 2$ sublattice structure, which enables the $l_s$ period spin stripe. In our calculations, we treat several tens of thousands of variational parameters for the largest systems. All the variational parameters are optimized by using the stochastic reconfiguration method [50].

To clarify physical properties of the ground states, we measured the spin structure factor $S_{\rm s}(\boldsymbol{q}) = \frac{1}{3N_s} \sum_{i,j} \langle \boldsymbol{S}_i \cdot \boldsymbol{S}_j \rangle e^{-i\boldsymbol{q}\cdot(\boldsymbol{r}_i - \boldsymbol{r}_j)}$, the charge structure factor $S_{\rm c}(\boldsymbol{q}) = \frac{1}{N_s} \sum_{i,j} \langle n_i n_j - \rho^2 \rangle e^{-i\boldsymbol{q}\cdot(\boldsymbol{r}_i - \boldsymbol{r}_j)}$, and the long-range part of $d_{x^2-y^2}$-wave SC correlation functions $P_d^\infty = \frac{1}{M} \sum_{|\boldsymbol{r}| \geqslant r_{\max}/2} P_d(\boldsymbol{r})$, where $M$ is the number of vectors satisfying $|\boldsymbol{r}| \geqslant r_{\max}/2$. Here, $\rho = \sum_{i,\sigma} \langle n_{i\sigma} \rangle / N_s$, $r_{\max} = L/\sqrt{2}$, and $P_d(\boldsymbol{r}) = \frac{1}{2N_s} \sum_i \langle \Delta^\dagger_d(\boldsymbol{r}) \Delta_d(\boldsymbol{r} + \boldsymbol{r}_i) + \Delta_d(\boldsymbol{r}) \Delta^\dagger_d(\boldsymbol{r} + \boldsymbol{r}_i) \rangle$, with $\Delta_d(\boldsymbol{r}_i) = \frac{1}{\sqrt{2}} \sum_{\boldsymbol{r}} g(\boldsymbol{r}) (c_{\boldsymbol{r}_i\uparrow} c_{\boldsymbol{r}_i+\boldsymbol{r}\downarrow} - c_{\boldsymbol{r}_i\downarrow} c_{\boldsymbol{r}_i+\boldsymbol{r}\uparrow})$. The form factor $g(\boldsymbol{r})$ is defined as $g(\boldsymbol{r}) = \delta_{r_x,0}(\delta_{r_y,1} + \delta_{r_y,-1}) - \delta_{r_y,0}(\delta_{r_x,1} + \delta_{r_x,-1})$, where $\boldsymbol{r} = (r_x, r_y)$. We define the spin/charge order parameter as $\Delta_{\rm S/C} = \sqrt{S_{\rm s/c}(\boldsymbol{q}_{\rm peak})/N_s}$, where $S_{\rm s/c}(\boldsymbol{q}_{\rm peak})$ represents the peak value of the spin/charge structure factor. We also define the SC order parameter as $\Delta_{\rm SC} = \sqrt{P_d^\infty}$.

## III. RESULTS

### A. Ground-state phase diagram of the $t - t'$ Hubbard model

The main results are summarized in Fig. 1, which shows the ground-state phase diagram in the $\delta$-$t'$ plane for $U/t = 10$. Throughout this paper, the stripe state with charge (spin) period $l_c$ ($l_s$) is denoted as C$l_c$S$l_s$ for simplicity. Charge-uniform states are obtained under the 2×2 sublattice structures, and energies are compared with inhomogeneous states obtained under longer sublattices. As shown in Fig. 1, charge-inhomogeneous states exist as the ground states in a wide range of $\delta$ for any $t'/t$. The wavelength of the charge $l_c$ becomes longer with the decrease of $\delta$, and eventually, the PS, whose wavelength is infinite, occurs between the antiferromagnetic insulator and

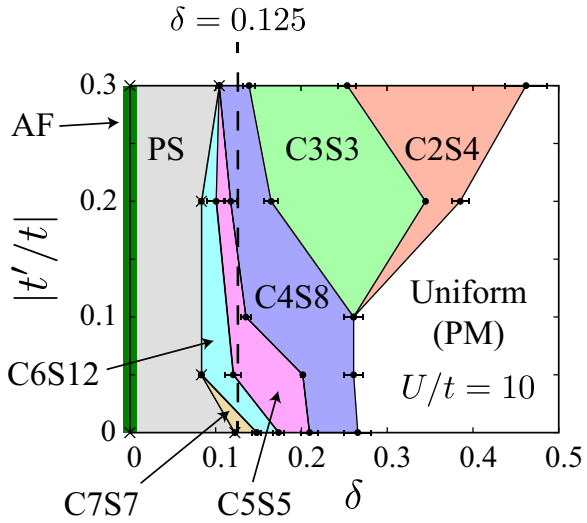


FIG. 1. Ground-state phase diagram of the Hubbard model on a square lattice for $U/t = 10$. Note that $t'/t$ is a negative value. At $\delta = 0$, the ground state is the antiferromagnetic (AF) Mott insulator (thick green line). Crosses indicate the calculated boundary of the phase separation (PS). Solid black circles represent the calculated boundaries of C$l_c$S$l_s$ stripe states, with $l_c$ and $l_s$ being the period for charge and spin, respectively. The dashed line shows $\delta = 0.125$. Solid lines and colored regions are guides for the eyes. In the white region, the ground state is a charge-uniform paramagnetic (PM) state.

a stripe state. For $-0.3 \leqslant t'/t \lesssim -0.15$, which is a realistic range of $t'/t$ for the cuprates, the ground state at $\delta = 1/8$ is the C4S8 state which has been observed in La-based cuprates [17,18]. However, charge-inhomogeneous states are stabilized even in the highly overdoped regime, and thus a uniform $d$-wave superconducting state does not appear as the ground state of the single-band Hubbard model *at strong coupling*. We will discuss our numerical results in comparison with the experiments in Sec. IV.

### B. Ground states and excited states

First, we show results for $t'/t = 0$ as the simplest model. Figure 2(a) shows the energies of uniform and stripe states with different periodicities as functions of hole-doping concentration $\delta = 1 - N/N_s$. We show evidence for the stripe long-range order described in Fig. 2(a) later in Fig. 4. From Fig. 2(a), we see that stripe states are the ground states below $\delta \approx 0.25$. The maximum value of the energy difference between uniform and stripe states is of the order of $\sim 0.01t$ at $\delta \approx 0.125$, which is consistent with the recent results by other numerical calculations such as the tensor network states [15,46]. By increasing the hole concentration, the wavelength of the charge $l_c$ becomes shorter. This is naturally related to the mean distance between holes, which decreases with increasing doping concentrations. Stripe states with $l_c \leqslant 3$ were not found as ground states.

To clarify the possibility of PS, we performed a Maxwell construction for the energy curve of the ground states [dashed line in Fig. 2(a)]. We find that a PS appears for $0 < \delta \leqslant 0.125$. This region is narrower than that obtained in the previous VMC study, where only uniform states were assumed [13]. Then we

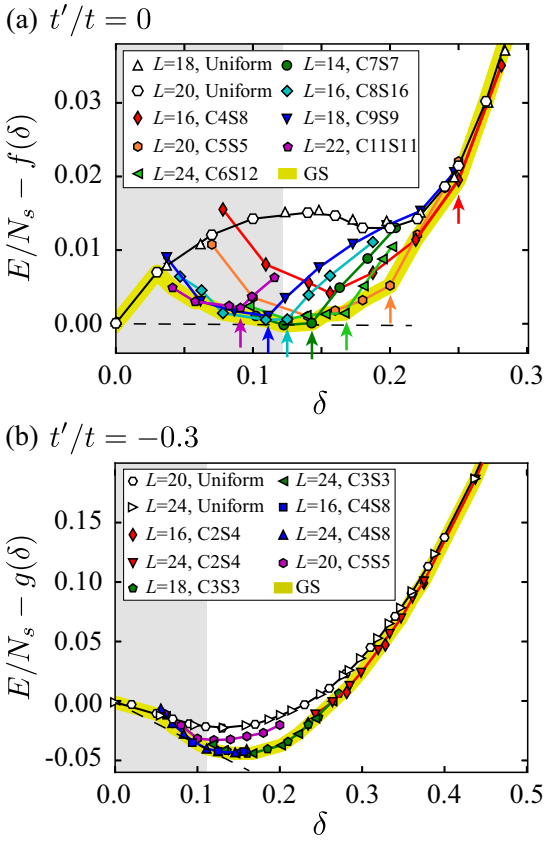


FIG. 2. Doping concentration dependence of energies for several different states in the two-dimensional Hubbard model with $U/t = 10$ at (a) $t'/t = 0$ and (b) $t'/t = -0.3$. A linear function $f(\delta) = -1.835\delta - 0.4211$ or $g(\delta) = -1.4\delta - 0.4211$ is subtracted for better visibility. For clarity, a thick yellow line represents the energies of the ground states. Types of states and system sizes are described in the legend. Error bars arising from the Monte Carlo sampling are all smaller than the symbol size. The dashed black line and gray region show the tangent line of the energy curve drawn from $\delta = 0$ and PS, respectively. In (a), commensurate fillings $\delta = 1/l_c$ are indicated by colored arrows.

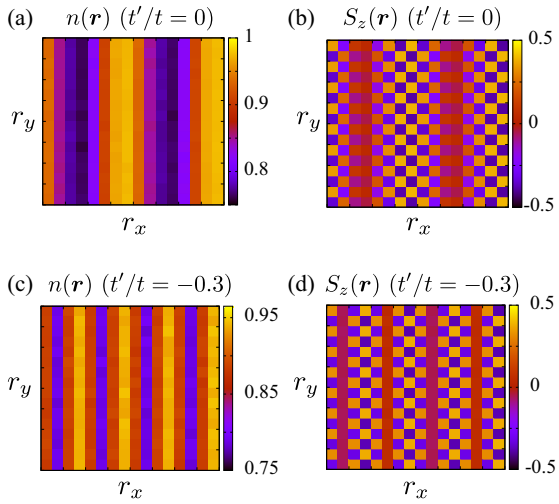


FIG. 3. Charge density $n(\boldsymbol{r}) = \langle n_{\boldsymbol{r}\uparrow} + n_{\boldsymbol{r}\downarrow} \rangle$ and spin density along the $z$ direction $S_z(\boldsymbol{r}) = 0.5 \langle n_{\boldsymbol{r}\uparrow} - n_{\boldsymbol{r}\downarrow} \rangle$ for the ground state for $L = 16$ and $U/t = 10$ at $\delta = 0.125$. The next-nearest-neighbor hoppings are (a) and (b) $t'/t = 0$ and (c) and (d) $t'/t = -0.3$. Note that the simulations were performed for finite-size systems. Nevertheless, the variational wave functions show translational symmetry breaking when the momentum projection is not operated. Although a better ground-state wave function is obtained after the momentum projection, the overlap of the two functions spatially translated with each other negligible in the size $L = 16$, and the order parameter is expected to be close to the thermodynamic limit.

conclude that the stripe states are stable ground states in the region $0.125 < \delta < 0.25$. At $\delta \approx 0.125$, several stripe states for $l_c = 6$–$8$ are nearly degenerate, which is also consistent with recent studies by other numerical methods [46]. The charge and spin configurations of the C8S16 state at $\delta = 0.125$ are plotted in Figs. 3(a) and 3(b), respectively.

Next, we show the results for $t'/t = -0.3$, which is a realistic value for the cuprate superconductors [48]. Figure 2(b) shows the hole-doping dependence of the energies for $U/t = 10$. We find an essential similarity to the case $t'/t = 0$, indicating the robust stability of the stripe ground state irrespective of the band structure. A quantitative difference is, however, that the stripe states as ground states extend in a wider region, $0.1 < \delta < 0.5$. Moreover, the ground state at $\delta = 0.125$ shows C4S8 order, which is consistent with the experiments of La-based cuprates [17,18]. The charge and spin configurations of the C4S8 ground state at $\delta = 0.125$ are shown in Figs. 3(c) and 3(d), respectively. This C4S8 state stably exists as the ground states for $0.11 \leqslant \delta \leqslant 0.15$, although it severely competes with other stripe order such as C3S3 and C5S5. The locking of stripe period has been recently observed in the scanning-tunneling-microscope experiment combined with the phase-resolved electronic structure visualization technique [29]. Below $\delta \sim 0.1$, a PS between antiferromagnetic and stripe states occurs as in the case of $t'/t = 0$.

### C. Spin, charge, and superconducting orders

The $\delta$ dependences of $\Delta_S^2$ and $\Delta_C^2$ for $t'/t = 0$ are shown in Figs. 4(a) and 4(b), respectively. We see that $\Delta_S^2$ decreases as $\delta$ increases. On the other hand, $\Delta_C^2$ has a dome structure around the maximum at $\delta \sim 0.1$. The domelike stripe order exists even after the extrapolation to the thermodynamic limit, as shown in Appendix B.

Figure 4(c) shows the $\delta$ dependence of $\Delta_{SC}^2$. We see that $\Delta_{SC}^2$ in the stripe states is substantially smaller than those of charge-uniform states. The previous VMC study showed that the strong superconductivity obtained by assuming charge uniformity emerges nearly in accordance with the region of the PS and therefore is mostly preempted by the PS [13]. In the present study, we have shown that if microscopic inhomogeneity is allowed, a large portion of the PS is compromised as the formation of stripes. The superconductivity is weakened by the stripe formation anyhow because of its character, where 1D-like carrier rich strips are weakly coupled by the interchain Josephson tunneling. However, it should be remarked that the uniform strongly SC state also survives as an excited state with the excitation energy on the order of $0.01t$ (in the cuprate scale ~10–100 K), as we see in Figs. 2(a) and 2(b). $\Delta_{SC}^2$ in the

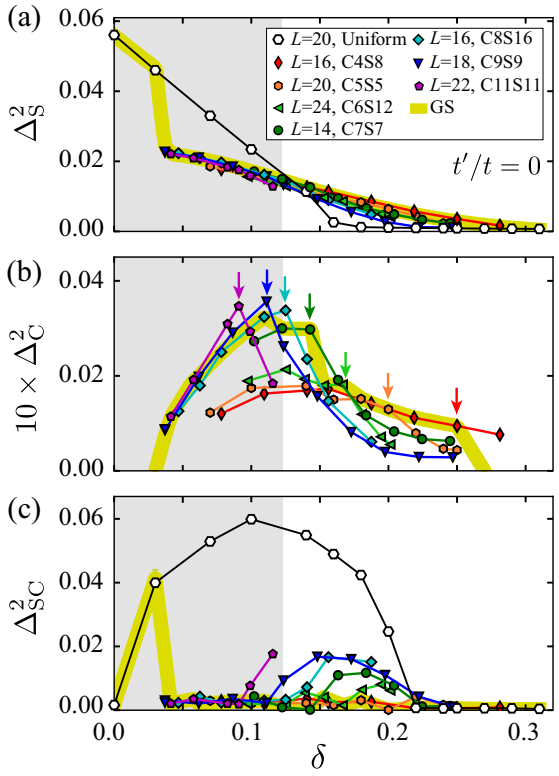


FIG. 4. The $\delta$ dependence of (a) $\Delta_S^2$, (b) $\Delta_C^2$, and (c) $\Delta_{SC}^2$ for $U/t=10$ and $t'/t=0$. Notations are the same as in Fig. 2(a). An enlarged view for $\Delta_{SC}^2$ is shown in Appendix A.

uniform state has a dome structure [13] similar to that of $\Delta_C^2$ in the ground state, as we see in Figs. 4(b) and 4(c).

Figure 5 plots physical quantities for the case of $t'/t=-0.3$, which are again similar to those in the case of $t'/t=0$.

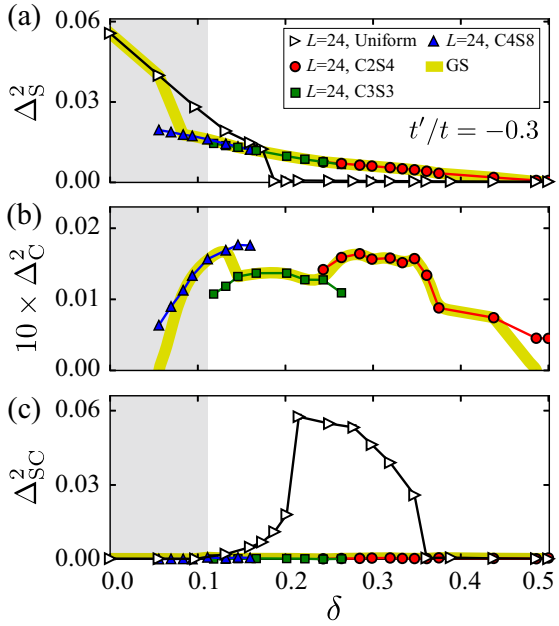


FIG. 5. The $\delta$ dependence of (a) $\Delta_S^2$, (b) $\Delta_C^2$, and (c) $\Delta_{SC}^2$ for $U/t=10$ and $t'/t=-0.3$. Notations are the same as in Fig. 2(b). An enlarged view for $\Delta_{SC}^2$ is shown in Appendix A.

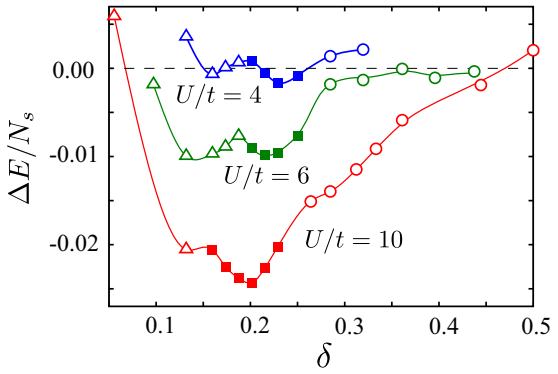


FIG. 6. Interaction dependence of the stability of uniform and inhomogeneous states (the energy difference $\Delta E = E_{\text{stripe}} - E_{\text{uniform}}$) for $t'/t=-0.3$. Here, $E_{\text{stripe}}$ and $E_{\text{uniform}}$ are the energies of stripe and uniform states, respectively. Circles, squares, and triangles show the energies of the C2S4, C3S3, and C4S8 stripes, respectively. Red, green, and blue symbols represent $\Delta E$ for $U/t=10$, 6, and 4, respectively. Curves are guides for the eyes.

Note that the stripe order parameters remain finite in the thermodynamic limit below $\delta\sim 0.4$ (see also Appendix B). However, in the experiments, the stripe state has been observed only below $\delta\sim 0.2$ [33]. This discrepancy will be discussed later.

### D. Interaction dependence for $t'/t=-0.3$

Finally, we show the interaction dependence of the energy difference between the uniform and inhomogeneous states for $t'/t=-0.3$ in Fig. 6. The stripe states are the ground states above $U/t\sim 4$, and the stripe phase expands with the increase in $U$. For $U/t=6$, the stripe and the uniform strongly SC states are nearly degenerate around $\delta\sim 0.3$. The stripe and uniform SC order parameters become smaller compared with those for $U/t=10$, but the $\delta$ dependence is similar, and we do not find a clear indication of PS. (See Appendix C.) At $U/t=4$, the charge-uniform state is nearly degenerate with the stripe state, but the order parameters for the stripe and SC are all nearly zero in both states, implying that the ground state is a paramagnetic metal. Although the stability changes, the stripe and SC orders have a similar trend in the dependences on $U$ and $\delta$.

## IV. DISCUSSION

The same trend between the stripe and SC orders is naturally understood because the emergent and strong effective attractive interaction of carriers, which arises from the originally repulsive interaction, generates both of the order. The stripe as a consequence of aggregation of carriers in real space and the strong-coupling superconductivity both require strong effective attraction of carriers. The effective attraction may have both static and retarded pieces. It is possible that the latter may be contributed by bosonic glues, including spin fluctuations [51–55], and reinforced by hidden-fermion excitations [56,57]. The static effective attraction is a direct consequence of the negative quadratic coefficient $b<0$ in the energy expansion $E=E_0+a\delta+b\delta^2+\cdots$, as seen in Figs. 2(a) and 2(b);

$b < 0$ is caused by the Mottness, where the kinetic energy decreases nonlinearly upon doping [13].

In the presence of realistic values of $t'/t$ and $U/t$ for cuprates, our calculations show a severe competition among stripe states with $l_c = 3$–7 below $\delta \sim 0.2$. The charge wavelengths $l_c = 3$–7 have been observed in a number of cuprates for $0.05 \lesssim \delta \lesssim 0.2$ [17–29]. The wavelength of charge $l_c = 4$ is consistent with the observations not only in La-based cuprates [17,18] but also in a Bi-based cuprate [29]. The charge inhomogeneity with $l_c = 5$–7 has been observed in La-based cuprates below $\delta \sim 0.1$ [19–21]. The wavelength $l_c = 3$ is close to the experimental observations for a Y-based cuprate [22–27]. The charge wavelengths observed in a single-layer Hg-based cuprate are $l_c \approx 3.58$ [23] and 4.35 [28], which is located within $l_c = 3$–5. Recent first-principles studies have shown that the single-layer Hg-based cuprate has weaker effective Coulomb interactions than the single-layer La-based cuprate [48,58]. Our results support these studies because the inhomogeneities become weaker with weakening of the interaction, which is consistent with the experiments where the charge order in the Hg-based cuprate is much weaker than that in the La-based cuprate [20,21,23].

The parameter values $t'/t = -0.3$ and $U/t = 10$ were proposed as realistic values for the cuprates [48,59,60]. However, our results show that the stripe phase is extended in a much wider range of $\delta$ compared with the experiments. On the other hand, by weakening $U/t$, the stripe order parameters and the energy difference between the stripe states and the uniform SC state becomes small. These results imply that an appropriate description of single-band effective Hamiltonians for cuprates is found in the region of intermediate on-site interactions rather than the strong-coupling region, at least in terms of the stability of the stripe and SC phases.

The reason why the $d$-wave SC ground state does not clearly appear, in contradiction to the experimental results, is speculated to be the oversimplification of the Hubbard models we studied. As recent numerical results are consistent with each other [46], the discrepancy does not seem to originate from the limitation of the accuracy of our calculations (see also the last paragraph of this section). In order to make a more quantitative and reliable comparison with experiments beyond our present analysis, we should analyze the *ab initio* effective Hamiltonians, which include long-range Coulomb interactions and hopping integrals and, if necessary, the electron-phonon coupling missing in the simplified Hubbard model. For example, in the *ab initio* single-band effective Hamiltonian for the Hg-based cuprate [48], the nearest-neighbor Coulomb interaction is about 20% of the on-site interaction. The third-nearest-neighbor hopping $t''$ in the effective Hamiltonian also has a non-negligible value of $t''/t \sim 0.15$ [48]. A tiny energy difference between the superconducting and stripe states is subject to be easily reversed by such realistic factors. We are now at a stage that allows quantitative comparisons between model (or even *ab initio*) calculations and the experimental results because of the achieved accuracy of the solver. The origin of the quantitative discrepancy will be discussed elsewhere based on first-principles studies.

One may be concerned about the accuracy of the present calculation. However, our trial wave function can be systematically improved by using methods such as the power Lanczos and/or tensor network [15,61–64]. These additional refinements indeed lower the energies. However, the energies are nearly equally lowered among competing states, and other physical quantities such as stripe and superconducting orders only slightly change [13,15]. (See also Appendix D.)

## V. SUMMARY

Our VMC calculations show stripe ground states of the Hubbard models irrespective of the amplitude of the next-nearest-neighbor hopping. The stability of the stripe states and the stripe order parameters substantially increase with increasing $U$ in the strong-coupling region beyond $U/t = 5$ and become extended in a wider range of hole-doping concentration with a domelike $\delta$ dependence. With increasing hole doping, the stripe period decreases. The stripe period is roughly proportional to the mean hole distance for $t'/t = 0.0$, whereas it is not for $t'/t = -0.3$. This detailed difference may be ascribed to the difference in the Fermi surface nesting vectors, especially in the antinodal region. This issue will be studied in future studies. The period at $t'/t = -0.3$ agrees with that observed in the experiments at $\delta = 0.125$.

In the static stripe ground states, the superconductivity is substantially suppressed. On the other hand, metastable excited states with uniform and strongly SC order, whose excitation energy is tiny ($\sim 0.01t$), appear with domelike $\delta$ dependence similar to the dome of charge stripe order. The superconducting order in both excited and ground states decreases for smaller $U/t$ and is numerically invisible for $U/t \lesssim 4$, which again has a trend essentially similar to the charge order.

The same trend between the SC and stripe states and their severe competition are a consequence of the strong effective attraction originating from the strong repulsive interaction. Understanding their common route and distinctions revealed here will help in designing ways to suppress the stripe and stabilize the SC state simultaneously. Some attempts have already been made [16,65], and extensive studies along this line are intriguing challenging issues for the future.

An interesting future issue is to more quantitatively analyze effective low-energy Hamiltonians of cuprates obtained from *ab initio* calculations [48] to understand the mechanisms and material dependence in light of the present severe competition. In particular, the validity of the single-band description has to be seriously examined because the present elucidation suggests a weaker correlation than the parameters proposed in the literature [48] if one sticks to the single-band description.

## ACKNOWLEDGMENTS

The authors thank the Supercomputer Center, the Institute for Solid State Physics, the University of Tokyo for the facilities. The calculations were performed by using the open-source software mVMC [66]. We acknowledge the computational resources of the K computer provided by the RIKEN Advanced Institute for Computational Science through the HPCI System Research project, as well as HPCI Strategic Programs for Innovative Research (SPIRE), the Computational Materials

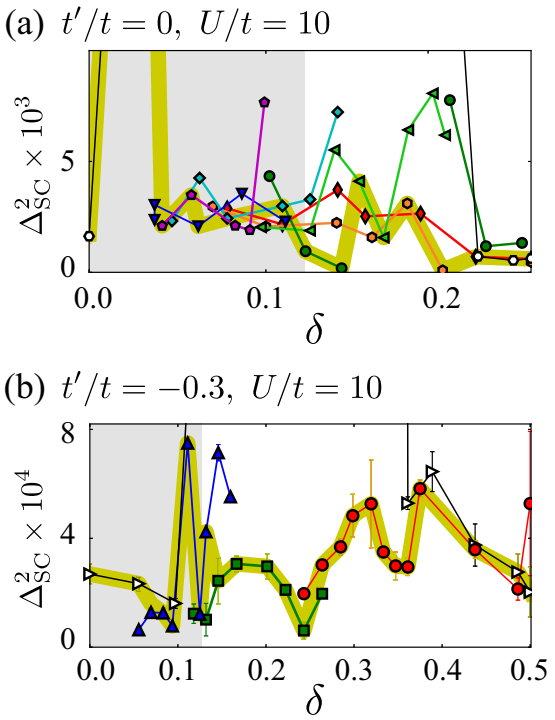


FIG. 7. Doping concentration dependence of the superconducting order parameter for $U/t = 10$ at (a) $t'/t = 0$ and (b) $t'/t = -0.3$. Notations in (a) and (b) are the same as in Figs. 4 and 5, respectively.

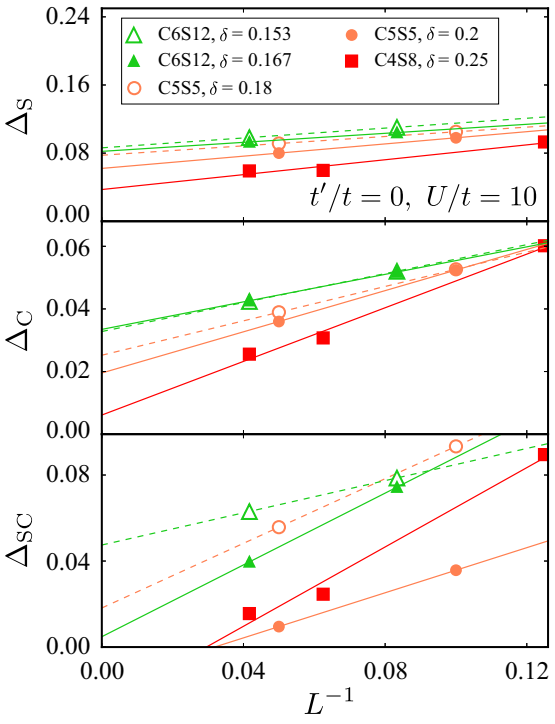


FIG. 8. System-size dependence of order parameters for $t'/t = 0$ and $U/t = 10$. In the legend, types of quantum states and hole concentrations are described. Solid symbols correspond to the commensurate fillings in which one hole fills per one charge-stripe unit cell. Solid and dashed lines represent the linear-extrapolation fittings by $a + bL^{-1}$.

Science Initiative (CMSI), and the social and scientific priority issue (Creation of new functional devices and high-performance materials to support next-generation industries, CDMSI) to be tackled using the post-K computer, under Projects No. hp130007, No. hp140215, No. hp150211, No. hp160201, and No. hp170263 supported by the Ministry of Education, Culture, Sports, Science and Technology, Japan (MEXT). This work was also supported by Grants-in-Aid for Scientific Research (Grants No. 22104010, No. 22340090, and No. 16H06345) from MEXT. K.I. was financially supported by a Grant-in-Aid for JSPS Fellows (Grant No. 17J07021) and the Japan Society for the Promotion of Science through the Program for Leading Graduate Schools (MERIT).

## APPENDIX A: ENLARGED VIEW OF $\delta$ DEPENDENCE OF $\Delta_{SC}$

Figures 7(a) and 7(b) show enlarged views of Figs. 4(c) and 5(c) in the main text, which plot the hole concentration dependence of the superconducting order parameters for $t'/t = 0$ and $t'/t = -0.3$, respectively. The maximum value of the SC order parameters for the ground states is of the order of

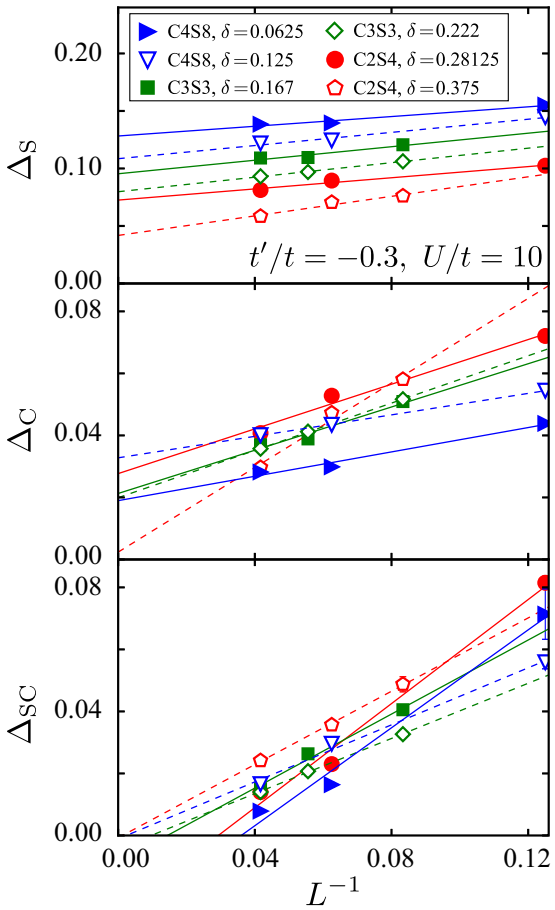


FIG. 9. System-size dependence of order parameters for $t'/t = -0.3$ and $U/t = 10$. In the legend, types of quantum states and hole concentrations are described. Solid and dashed lines represent the linear-extrapolation fittings.

$10^{-4}$–$10^{-3}$ at most, which is much smaller than that of the uniform excited state.

## APPENDIX B: SIZE DEPENDENCE OF STRIPE AND SUPERCONDUCTING ORDER PARAMETERS FOR STRIPE STATES

To clarify the thermodynamic properties of the ground states, we show the size dependence of physical quantities for $t'/t = 0$ and $U/t = 10$ within the stripe ground state at several doping concentrations in Fig. 8. Here, following the convention in the literature [67], we estimate the extrapolated order parameter $\Delta$ by fitting several points with $a + bL^{-1}$. Even when we employ the scaling $a' + b'L^{-1/2}$, the results do not essentially change. Figure 8 shows that both the spin and charge order parameters remain finite even after extrapolations below $\delta \sim 0.2$. At commensurate fillings, one hole fills in a one-charge wavelength, i.e., $\delta = 1/l_c$. The bottom panel of Fig. 8 shows, in the thermodynamic limit, clear stronger suppression of long-range superconducting order at commensurate fillings $\delta = 1/l_c$ than the case $\delta \neq 1/l_c$, which is incommensurate to the stripe period. In the latter incommensurate fillings, the superconducting order likely remains nonzero in the thermodynamic limit.

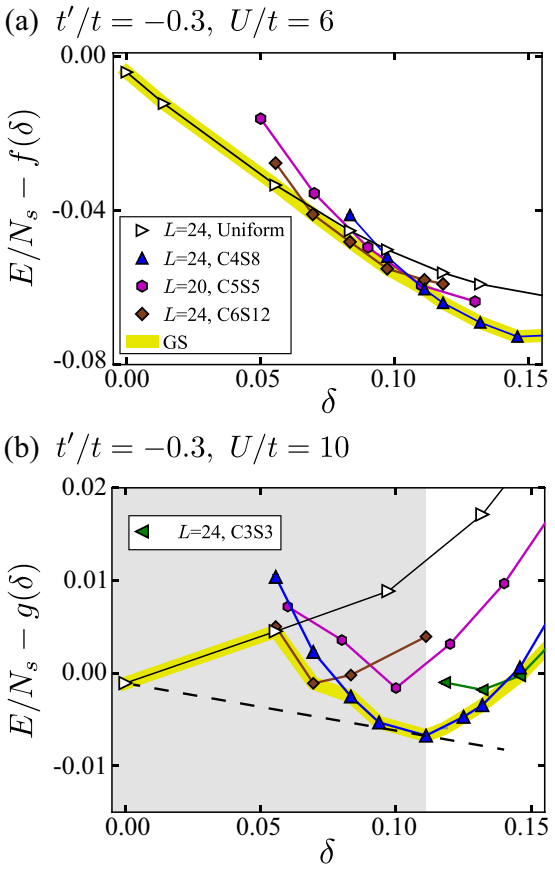


FIG. 10. Doping dependence of the energy of several different states for $t'/t = -0.3$ below $\delta = 0.15$. We set $f(\delta) = -0.8\delta - 0.640$ and $g(\delta) = -1.7\delta - 0.4211$. Types of states and system sizes are described in the legend. For clarity we draw a thick yellow line for the energies of the ground states for $L = 24$. The dashed black line and gray region show the tangent line of the energy curve drawn from the $\delta = 0$ ground state and PS, respectively.

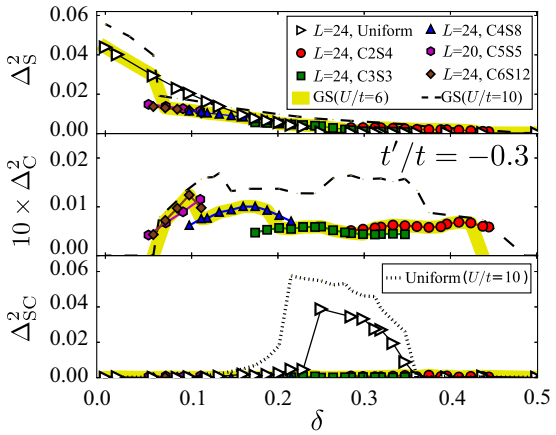


FIG. 11. Doping concentration dependence of squared order parameters for spin (top panel) and charge (middle panel) stripes and superconductivity (bottom panel) for $U/t = 6$ and $t'/t = -0.3$. Dashed and dotted curves represent the results of the ground states and the charge-uniform state for $U/t = 10$ for comparison, respectively. Notations are the same as Fig. 5.

We also show size dependences of physical quantities for $t'/t = -0.3$ in Fig. 9. As we mentioned in the main text, the extrapolated values of stripe orders have nonzero values below $\delta \sim 0.4$. On the other hand, we do not find any positive extrapolated values of the SC order parameter at this stage, which is different from the case of $t'/t = 0$. To understand this difference, we need further analysis of the size dependence of the SC order parameter and its doping dependence in the thermodynamic limit for both $t'/t = 0$ and $t'/t = -0.3$, but this is left for a future study.

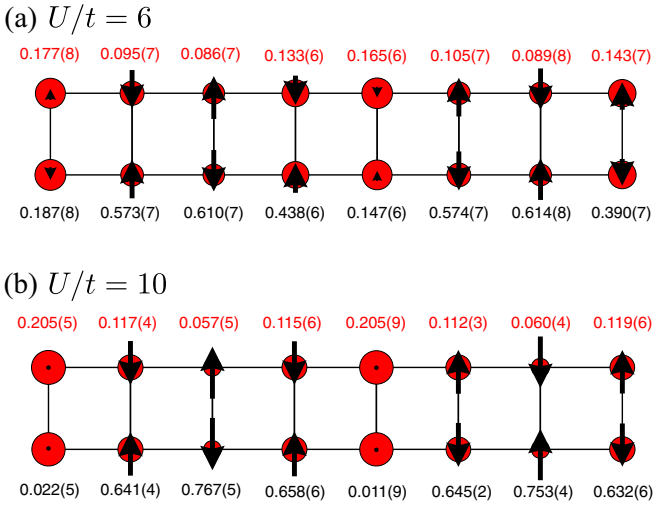


FIG. 12. Spin density along the $z$ direction $S_i^z = \langle n_{i\uparrow} - n_{i\downarrow} \rangle$ and hole density $1 - \langle n_i \rangle = 1 - \langle n_{i\uparrow} + n_{i\downarrow} \rangle$ for $t'/t = -0.3$ at $\delta = 0.125$ for the ground state with C4S8 for $L = 24$. The radius of every red circle is proportional to the hole density $1 - \langle n_i \rangle$. The length of every black arrow is proportional to the amplitude of the spin density $|S_i^z|$. The values of $|S_i^z|$ and $1 - \langle n_i \rangle$ averaged over the $y$ direction are shown above and below the plots, respectively. The number in parentheses represents the error on the last digit.

TABLE I. Energies per site of competing states obtained from the VMC and first Lanczos calculations for several system sizes $L$ and hole-doping concentrations $\delta$ at $U/t = 10$ and $t'/t = 0$. The number in parentheses represents the error on the last digit.

| $L$ | $\delta$ | State | VMC | First Lanczos |
|---|---|---|---|---|
| 20 | 0.180 | Uniform | −0.7384(2) | −0.7591(4) |
| 20 | 0.180 | C5S5 | −0.74820(4) | −0.7639(8) |
| 14 | 0.143 | Uniform | −0.6665(5) | −0.6900(7) |
| 14 | 0.143 | C7S7 | −0.68315(5) | −0.6992(3) |
| 16 | 0.109 | Uniform | −0.60744(9) | −0.6272(4) |
| 16 | 0.109 | C8S16 | −0.62232(4) | −0.6377(1) |

## APPENDIX C: PHYSICAL QUANTITIES FOR $t'/t = -0.3$ AND $U/t = 6$

Figure 10 compares the hole-doping dependence of the energies between $U/t = 6$ and $U/t = 10$ below $\delta \sim 0.15$. We do not find an evidence for the PS between the antiferromagnetic state and the stripe state at $U/t = 6$, where a tangent line from $\delta = 0$ to the other point ($\delta > 0$) of the energy curve cannot be drawn, distinct from the case $U/t = 10$.

Figure 11 plots the $\delta$ dependence of the spin, charge, and superconducting order parameters for $U/t = 6$ and $t'/t = -0.3$. We see that the results are qualitatively similar to those for the case of $U/t = 10$, but the stripe order parameters become smaller. This means that the inhomogeneity is weakened by the decrease in the on-site interaction. This tendency is also seen in Fig. 12, where the electron distribution in real space is depicted. The superconductivity in the uniform excited states has the same trend as the case of the stripe orders. At $U/t = 4$, the stripe and superconducting orders are scaled to zero within the numerical accuracy.

## APPENDIX D: POWER LANCZOS METHOD

The power Lanczos method is one of the systematic ways to improve a trial wave function in the VMC method [61]. In the $N$-th power Lanczos method, we operate the Hamiltonian to the optimized trial wave function $|\psi_{\rm opt}\rangle$ as

$$|\psi^{(N)}\rangle = \left(1 + \sum_{n=1}^{N} \alpha_n \mathcal{H}^n\right) |\psi_{\rm opt}\rangle\,, \tag{D1}$$

where $\alpha_n$ are the variational parameters. We use the first-step Lanczos method ($N = 1$) since the numerical costs grow exponentially with increasing $N$.

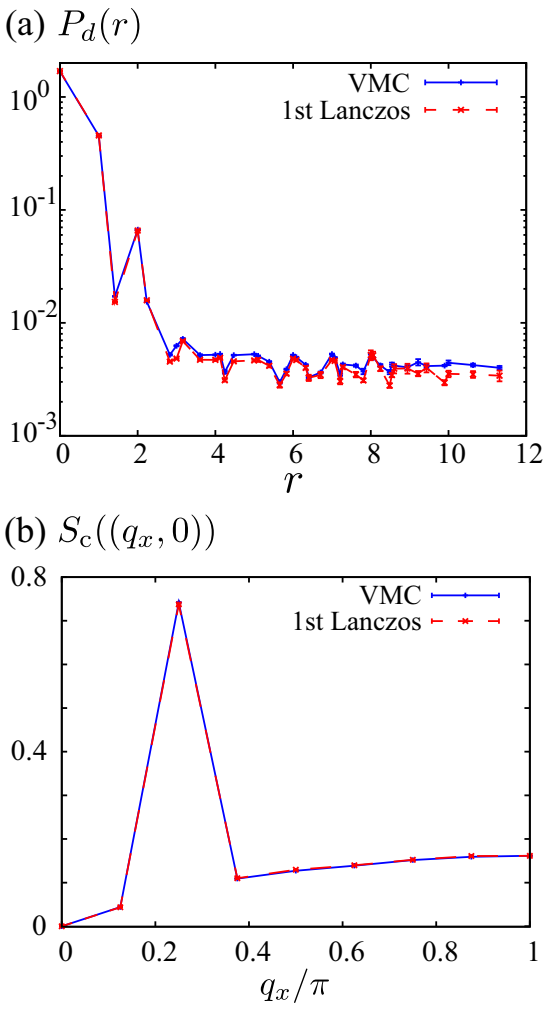


FIG. 13. (a) Superconducting correlation function $P_d(r)$ and (b) charge structure factor $S_c(\boldsymbol{q}_{\rm peak})$ at $\boldsymbol{q}_{\rm peak} = (q_x, 0)$ of the C8S16 state for $L = 16$, $U/t = 10$, and $t'/t = 0$ at $\delta \approx 0.11$. The solid blue line and dashed red line are the results obtained by using the VMC method and the first-step Lanczos method, respectively.

Table I shows the energies of competing states for various doping concentrations $\delta$. The Lanczos method improves the energies of competing states but does not change the character of the ground states and only slightly alters physical properties. We have checked the effects of the Lanczos operation on other physical quantities such as the superconducting correlation function and the charge structure factor. However, they are only slightly changed, as shown in Fig. 13.

[1] J. G. Bednorz and K. A. Müller, Z. Phys. **64**, 189 (1986).
[2] N. Furukawa and M. Imada, J. Phys. Soc. Jpn. **61**, 3331 (1992).
[3] N. Furukawa and M. Imada, J. Phys. Soc. Jpn. **62**, 2557 (1993).
[4] J. Zaanen and O. Gunnarsson, Phys. Rev. B **40**, 7391 (1989).
[5] V. J. Emery, S. A. Kivelson, and H. Q. Lin, Phys. Rev. Lett. **64**, 475 (1990).
[6] S. A. Kivelson and V. J. Emery, Synth. Met. **80**, 151 (1996).
[7] S. R. White and D. J. Scalapino, Phys. Rev. B **61**, 6320 (2000).
[8] A. Himeda, T. Kato, and M. Ogata, Phys. Rev. Lett. **88**, 117001 (2002).
[9] P. Corboz, S. R. White, G. Vidal, and M. Troyer, Phys. Rev. B **84**, 041108 (2011).
[10] D. J. Scalapino and S. R. White, Phys. C (Amsterdam, Neth.) **481**, 146 (2012).

[11] P. Corboz, T. M. Rice, and M. Troyer, Phys. Rev. Lett. **113**, 046402 (2014).
[12] M. Capone and G. Kotliar, Phys. Rev. B **74**, 054513 (2006).
[13] T. Misawa and M. Imada, Phys. Rev. B **90**, 115137 (2014).
[14] J. Otsuki, H. Hafermann, and A. I. Lichtenstein, Phys. Rev. B **90**, 235132 (2014).
[15] H.-H. Zhao, K. Ido, S. Morita, and M. Imada, Phys. Rev. B **96**, 085103 (2017).
[16] K. Ido, T. Ohgoe, and M. Imada, Sci. Adv. **3**, e1700718 (2017).
[17] J. M. Tranquada, B. J. Sternlieb, J. D. Axe, Y. Nakamura, and S. Uchida, Nature (London) **375**, 561 (1995).
[18] J. M. Tranquada, J. D. Axe, N. Ichikawa, A. R. Moodenbaugh, Y. Nakamura, and S. Uchida, Phys. Rev. Lett. **78**, 338 (1997).
[19] K. Yamada, C. H. Lee, K. Kurahashi, J. Wada, S. Wakimoto, S. Ueki, H. Kimura, Y. Endoh, S. Hosoya, G. Shirane *et al.*, Phys. Rev. B **57**, 6165 (1998).
[20] M. Hücker, M. V. Zimmermann, Z. J. Xu, J. S. Wen, G. D. Gu, and J. M. Tranquada, Phys. Rev. B **87**, 014501 (2013).
[21] J. Fink, V. Soltwisch, J. Geck, E. Schierle, E. Weschke, and B. Büchner, Phys. Rev. B **83**, 092503 (2011).
[22] G. Ghiringhelli, M. Le Tacon, M. Minola, S. Blanco-Canosa, C. Mazzoli, N. B. Brookes, G. M. De Luca, A. Frano, D. G. Hawthorn, F. He *et al.*, Science **337**, 821 (2012).
[23] W. Tabis, Y. Li, M. Le Tacon, L. Braicovich, A. Kreyssig, M. Minola, G. Dellea, E. Weschke, M. J. Veit, M. Ramazanoglu *et al.*, Nat. Commun. **5**, 5875 (2014).
[24] R. Comin, R. Sutarto, E. H. da S. Neto, L. Chauviere, R. Liang, W. N. Hardy, D. A. Bonn, F. He, G. A. Sawatzky, and A. Damascelli, Science **347**, 1335 (2015).
[25] R. Comin, R. Sutarto, F. He, E. H. da S. Neto, L. Chauviere, A. Fraño, R. Liang, W. N. Hardy, D. A. Bonn, Y. Yoshida *et al.*, Nat. Mater. **14**, 796 (2015).
[26] E. M. Forgan, E. Blackburn, A. T. Holmes, A. K. R. Briffa, J. Chang, L. Bouchenoire, S. D. Brown, R. Liang, D. Bonn, W. N. Hardy *et al.*, Nat. Commun. **6**, 10064 (2015).
[27] Y. Y. Peng, M. Salluzzo, X. Sun, A. Ponti, D. Betto, A. M. Ferretti, F. Fumagalli, K. Kummer, M. Le Tacon, X. J. Zhou *et al.*, Phys. Rev. B **94**, 184511 (2016).
[28] G. Campi, A. Bianconi, N. Poccia, G. Bianconi, L. Barba, G. Arrighetti, D. Innocenti, J. Karpinski, N. D. Zhigadlo, S. M. Kazakov *et al.*, Nature (London) **525**, 359 (2015).
[29] A. Mesaros, K. Fujita, S. D. Edkins, M. H. Hamidian, H. Eisaki, S. Uchida, J. C. S. Davis, M. J. Lawler, and E.-A. Kim, Proc. Natl. Acad. Sci. USA **113**, 12661 (2016).
[30] H. Eduardo, S. Neto, P. Aynajian, A. Frano, R. Comin, E. Schierle, E. Weschke, A. Gyenis, J. Wen, J. Schneeloch *et al.*, Science **343**, 393 (2014).
[31] K. Fujita, M. H. Hamidian, S. D. Edkins, C. K. Kim, Y. Kohsaka, M. Azuma, M. Takano, H. Takagi, H. Eisaki, S. Uchida *et al.*, Proc. Natl. Acad. Sci. USA **111**, E3026 (2014).
[32] B. Keimer, S. A. Kivelson, M. R. Norman, S. Uchida, and J. Zaanen, Nature (London) **518**, 179 (2015).
[33] R. Comin and A. Damascelli, Annu. Rev. Condens. Matter Phys. **7**, 369 (2016).
[34] T. Giamarchi and C. Lhuillier, Phys. Rev. B **43**, 12943 (1991).
[35] H. Yokoyama, M. Ogata, Y. Tanaka, K. Kobayashi, and H. Tsuchiura, J. Phys. Soc. Jpn. **82**, 014707 (2013).
[36] M. Aichhorn, E. Arrigoni, M. Potthoff, and W. Hanke, Phys. Rev. B **76**, 224509 (2007).
[37] S. S. Kancharla, B. Kyung, D. Sénéchal, M. Civelli, M. Capone, G. Kotliar, and A.-M. S. Tremblay, Phys. Rev. B **77**, 184516 (2008).
[38] C.-C. Chang and S. Zhang, Phys. Rev. B **78**, 165101 (2008).
[39] C.-C. Chang and S. Zhang, Phys. Rev. Lett. **104**, 116402 (2010).
[40] E. Khatami, K. Mikelsons, D. Galanakis, A. Macridin, J. Moreno, R. T. Scalettar, and M. Jarrell, Phys. Rev. B **81**, 201101 (2010).
[41] G. Sordi, P. Sémon, K. Haule, and A.-M. S. Tremblay, Phys. Rev. Lett. **108**, 216401 (2012).
[42] E. Gull and A. J. Millis, Phys. Rev. B **86**, 241106 (2012).
[43] B.-X. Zheng and G. K.-L. Chan, Phys. Rev. B **93**, 035126 (2016).
[44] J. P. F. LeBlanc, A. E. Antipov, F. Becca, I. W. Bulik, G. K.-L. Chan, C.-M. Chung, Y. Deng, M. Ferrero, T. M. Henderson, C. A. Jiménez-Hoyos *et al.*, Phys. Rev. X **5**, 041041 (2015).
[45] L. F. Tocchio, H. Lee, H. O. Jeschke, R. Valentí, and C. Gros, Phys. Rev. B **87**, 045111 (2013).
[46] B.-X. Zheng, C.-M. Chung, P. Corboz, G. Ehlers, M.-P. Qin, R. M. Noack, H. Shi, S. R. White, S. Zhang, and G. K.-L. Chan, Science **358**, 1155 (2017).
[47] L. F. Tocchio, F. Becca, and S. Sorella, Phys. Rev. B **94**, 195126 (2016).
[48] M. Hirayama, Y. Yamaji, T. Misawa, and M. Imada, arXiv:1708.07498.
[49] D. Tahara and M. Imada, J. Phys. Soc. Jpn. **77**, 114701 (2008).
[50] S. Sorella, Phys. Rev. B **64**, 024512 (2001).
[51] T. A. Maier, D. Poilblanc, and D. J. Scalapino, Phys. Rev. Lett. **100**, 237001 (2008).
[52] B. Kyung, D. Sénéchal, and A.-M. S. Tremblay, Phys. Rev. B **80**, 205109 (2009).
[53] M. Civelli, Phys. Rev. Lett. **103**, 136402 (2009).
[54] D. J. Scalapino, E. Loh, and J. E. Hirsch, Phys. Rev. B **34**, 8190 (1986).
[55] K. Miyake, S. Schmitt-Rink, and C. M. Varma, Phys. Rev. B **34**, 6554 (1986).
[56] S. Sakai, M. Civelli, and M. Imada, Phys. Rev. Lett. **116**, 057003 (2016).
[57] S. Sakai, M. Civelli, and M. Imada, Phys. Rev. B **94**, 115130 (2016).
[58] S. W. Jang, H. Sakakibara, H. Kino, T. Kotani, K. Kuroki, and M. J. Han, Sci. Rep. **6**, 33397 (2016).
[59] M. S. Hybertsen, E. B. Stechel, M. Schluter, and D. R. Jennison, Phys. Rev. B **41**, 11068 (1990).
[60] K. Tsutsui, T. Tohyama, and S. Maekawa, Phys. Rev. Lett. **83**, 3705 (1999).
[61] E. S. Heeb and T. M. Rice, Z. Phys. **90**, 73 (1993).
[62] E. Neuscamman, C. J. Umrigar, and G. K.-L. Chan, Phys. Rev. B **85**, 045103 (2012).
[63] C.-P. Chou, F. Pollmann, and T.-K. Lee, Phys. Rev. B **86**, 041105 (2012).
[64] O. Sikora, H.-W. Chang, C.-P. Chou, F. Pollmann, and Y.-J. Kao, Phys. Rev. B **91**, 165113 (2015).
[65] T. Misawa, Y. Nomura, S. Biermann, and M. Imada, Sci. Adv. **2**, e1600664 (2016).
[66] T. Misawa, S. Morita, K. Yoshimi, M. Kawamura, Y. Motoyama, K. Ido, T. Ohgoe, M. Imada, and T. Kato, arXiv:1711.11418.
[67] F. F. Assaad and I. F. Herbut, Phys. Rev. X **3**, 031010 (2013).